

Accepted Manuscript

Discovery of *N*-hydroxy-3-alkoxybenzamides as direct acid sphingomyelinase inhibitors using a ligand-based pharmacophore model

Kan Yang, Keyi Nong, Qinlan Gu, Jibin Dong, Jinxin Wang



PII: S0223-5234(18)30308-8

DOI: [10.1016/j.ejmech.2018.03.065](https://doi.org/10.1016/j.ejmech.2018.03.065)

Reference: EJMECH 10330

To appear in: *European Journal of Medicinal Chemistry*

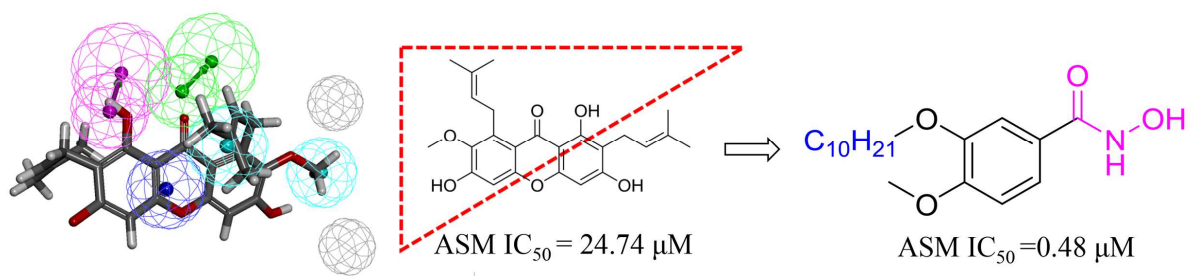
Received Date: 23 January 2018

Revised Date: 20 March 2018

Accepted Date: 21 March 2018

Please cite this article as: K. Yang, K. Nong, Q. Gu, J. Dong, J. Wang, Discovery of *N*-hydroxy-3-alkoxybenzamides as direct acid sphingomyelinase inhibitors using a ligand-based pharmacophore model, *European Journal of Medicinal Chemistry* (2018), doi: 10.1016/j.ejmech.2018.03.065.

This is a PDF file of an unedited manuscript that has been accepted for publication. As a service to our customers we are providing this early version of the manuscript. The manuscript will undergo copyediting, typesetting, and review of the resulting proof before it is published in its final form. Please note that during the production process errors may be discovered which could affect the content, and all legal disclaimers that apply to the journal pertain.



ACCEPTED MANUSCRIPT

Discovery of *N*-Hydroxy-3-alkoxybenzamides as Direct Acid Sphingomyelinase Inhibitors Using a Ligand-Based Pharmacophore Model

Kan Yang¹, Keyi Nong¹, Qinlan Gu², Jibin Dong^{3*}, Jinxin Wang^{1*}

¹Jiangsu Key Laboratory of Drug Design and Optimization, Department of Medicinal Chemistry, School of Pharmacy, China Pharmaceutical University, Nanjing 210009, China

²Senior Vocational School, China Pharmaceutical University, Nanjing 210009, China

³Department of Biochemistry, School of Pharmacy, Fudan University, Shanghai 201203, China.

Corresponding author E-mail address: jinxinwangcpu@126.com; jbdong@shmu.edu.cn

Abstract

Acid sphingomyelinase (ASM) has been shown to be involved in many physiological processes, emerging to be a promising drug target. In this study, we constructed a ligand-based pharmacophore model of ASM inhibitors and applied this model to optimize the lead compound α -mangostin, a known inhibitor of ASM. 23 compounds were designed and evaluated *in vitro* for ASM inhibition, of these, 10 compounds were found to be more potent than α -mangostin. This high hit ratio confirmed that the presented model is very effective and practical. The most potent hit, **1c**, was found to selectively and competitively inhibit the enzyme and inhibit the generation of ceramide in a dose-dependent manner. Furthermore, **1c** showed favorable anti-apoptosis and anti-inflammatory activity. Interactions with key residues and the Zn²⁺ cofactor of **1c** were found by docking simulation. These results provide promising leads and important guidance for further development of efficient ASM inhibitors and drug candidates.

Keywords: acid sphingomyelinase; inhibitors; pharmacophore model; anti-apoptosis; anti-inflammatory

Introduction

Acid sphingomyelinase (ASM) is a zinc-dependent phosphodiesterase that catalyzes the conversion of sphingomyelin (SM) into ceramide (Cers) and phosphocholine at the cytomembrane or intralysosomal membranes. Cers, which serves as a precursor for the synthesis of complex sphingolipids and as a versatile signalling lipid in the regulation of fundamental processes of cell proliferation and death, has been characterized in recent genomic and lipidomic research as the central signaling and metabolic relay among sphingolipids [1-3]. Furthermore, the extreme hydrophobicity of Cers leads to the formation of Cers-enriched membrane microdomains that play an essential role in transmembrane signaling [4, 5]. The excessively activated ASM-Cers system can lead to inflammation [6-8], apoptosis [9-11], insulin resistance [3], and mitochondrial dysfunction [12] under pathologic conditions. Accordingly, in patients with cardiovascular disease, diabetes or major depression, the activity of ASM was found to be significantly higher than in normal individuals [13-15]. Higher Cers level was also found in cystic fibrosis (CF) patients due to the higher ratio of ASM / acid ceramidase [16]. Functional inhibitors of ASM such as amitriptyline and imipramine were found to prevent or slow the progression of such pathologies in various animal studies [17-19]. Meanwhile, a direct inhibitor ARC39 was recently reported to attenuate murine acute lung injury [20]. On the basis of these significant results, ASM has received much attention as an attractive therapeutic target for treating Cers-associated diseases, especially lung diseases [1], metabolic disorders [3, 21], and central nervous system disease [22, 23]. In several phase-II trials for CF, amitriptyline showed good therapeutic effects by inhibiting ASM, which reduced Cers concentrations in lungs [24-26].

In most reported biological studies, the activity of ASM was controlled by genetic deletion or indirect inhibition by certain antidepressants that lead to its degradation. At present, direct inhibitors were needed to further examine and verify its pharmacological potential as a drug target. However, only a limited number of direct inhibitors have been reported, including analogues of SM [27], bisphosphonates [28], phosphatidylinositol-3,5-bisphosphates derivatives [29-31], benzopyrone derivatives [32], xanthone derivatives [33, 34]. The usefulness of these molecules has been

limited by their lability towards phospholipases and their difficulty in penetrating biological membranes [35]. Therefore, there is a great need to identify structurally distinct and more efficient small molecules as direct inhibitors.

There was no available 3D structure of ASM in our early inhibitors studies. We had constructed an initial ligand-based pharmacophore model to provide insights into design and development of ASM inhibitors. Directed by the model, we focused our investigations on synthesizing derivatives of α -mangostin, a known competitive inhibitor of ASM ($IC_{50} = 14.1 \mu M$) derived from pericarps of the mangosteen fruit [36]. However, moderate deviation was observed between the predicted and experimental activities of the synthesized derivatives. This discrepancy may be due to the four features of the original model were less and too closely ranged: one hydrogen bond acceptor (HBA), one hydrogen bond donor (HBD), and two hydrophobic groups (HY), indicating the model was not ideal for further application in the development of ASM inhibitors [37].

With newly obtained inhibitors in hand [33], herein we extended the training set and optimized the pharmacophore model, taking advantage of more accurate features: one HBA, one HBD, two HYS, one negatively ionizable group (NI), and two excluded volumes (EV). The model was used to analyze the pharmacophores of α -mangostin. As a result, a novel class of ASM direct inhibitors were successfully discovered through pharmacophore-guided and experience-based structural simplification and optimization of α -mangostin, which involved an interesting transformation from the natural structure to small-molecule inhibitors. Structure-activity relationship analysis provided a detailed insight into structural requirements for ASM activity of the new scaffold. In order to explore the impact on Cers level when ASM was directly inhibited, the most active compound **1c** was selected to test for inhibition of Cers generation. We also favorably included investigations of **1c** as a promising anti-apoptosis and anti-inflammatory agent by detection of cell viability and the inhibition of the related inflammatory factor, including IL-6 and IL-8.

It is encouraging that three research groups have reported resolution of the crystal structure of ASM [38-40]. Thus, the potential binding modes between the compound and the protein were intensively analyzed by docking simulations, which will provide more beneficial information for further design of inhibitors.

Results and discussion

Generation and validation of pharmacophore models.

The ligand-based 3D pharmacophore model was generated using 21 training set molecules (Table S1) in the 3D QSAR Pharmacophore Generation protocol of Discovery Studio 3.0 (DS 3.0). The protocol uses the Catalyst HypoGen algorithm and generated ten pharmacophore hypotheses, among which Hypo 1 was identified as the best pharmacophore model characterized based on the rank values (Table S2). The expected pharmacophore model showed a total cost (97.039) close to the fixed cost (84.339) and significant difference (91.655) between null and total cost. Moreover, Hypo 1 showed the lowest root mean square deviation (RMSD, 1.066) and best correlation coefficient (0.948). Besides this, Hypo-1 estimated the highest fit value of 8.33 for the most active compounds and 4.42 for the least active compounds (Table S4). All these data suggest the model is capable of predicting the activity of ASM inhibitors. This model consists of one HBA, one HBD, two HYs, one NI, and two EVs (Figure 1A).

Validation of the pharmacophore model was carried out by using the training and test set compounds (Table S3). Experimental and estimated activities data for the test set compounds are shown in Figure S1 and Table S5. As expected, Hypo-1 explained well the activity variation among these compounds with considerably low RMS error. An error of less than 10 means that the difference in the estimated IC_{50} value and the experimental IC_{50} value is less than one order of magnitude. In addition, there was a good correlation coefficient ($R^2 = 0.8557$) for the test set. The Fischer's randomization test at 95% confidence level was used to evaluate the statistical significance of the model by scrambling the activities of compounds in the training set. Results confirm that the cost value of Hypo 1 is lower than the 19 randomly generated trials and there is a 95% chance that the Hypo1 represents a true correlation for the training set compounds (Figure S1). Thus, the Hypo 1 model is superior and was not generated by chance.

Mapping of the most active compound **S1** in the training set (experimental activity: $IC_{50} = 0.02 \mu\text{M}$ and predicted activity: $IC_{50} = 0.016 \mu\text{M}$) revealed that all the features were mapped to the pharmacophore model with least displacement from the centroid. As shown in Figure 1B, the only amino group of **S1** mapped with the HBD of Hypo-1 and the hydrophobic chain mapped to the two HY groups. One oxygen atom from the PO_3H_2 group mapped well with the HBA feature, while the other PO_3H_2 group

mapped with the NI group. However, the less active compound **S21** (experimental activity: $IC_{50} = 196.6 \mu M$ and predicted activity: $IC_{50} = 132.2 \mu M$) only mapped to the two HY groups (Figure 1C). It is noteworthy that ASM is fully or partially dependent on Zn^{2+} for enzymatic activity [41]. The bisphosphonates in the training set with a hydroxy or amino group were reported to form stable tridentate complexes with Zn^{2+} ions at the catalytic center of ASM [28]. Meanwhile, with respect to the mapping of compound **S1** with the pharmacophore model, we hypothesized that the NI together with HBA and HBD function as a Zn^{2+} binding site.

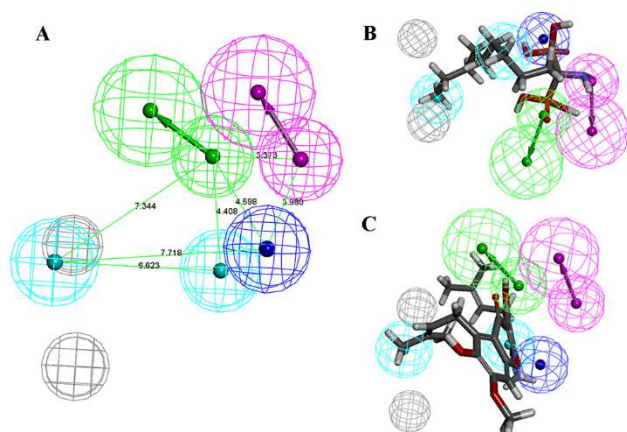


Figure 1. Hypo1 and its mapping to the most active and least active compounds from training set. (A) The topological features of Hypo1: green: HBA, magenta: HBD, cyan: HY, blue: NI, gray: EV. (B) The most potent compound **S1** mapped with Hypo 1. (C) The less active compound **S21** mapped with Hypo 1.

Design of novel ASM inhibitors

We mapped α -mangostin to Hypo 1 and found that only part of the molecule was matched, as shown in the red triangle in Figure 2. The carbonyl and hydroxyl at C-1 were mapped to the HBA and HBD, respectively, with little deviation. The methoxy at C-7 and the prenyl group at C-8 were mapped with the two HY groups while the NI group was not included. A previously study had also confirmed that xanthone with a prenyl group only at the C-8 residue maintained comparable activity to that of α -mangostin [34]. Thus, we deleted the groups outside the triangle in the structure of α -mangostin (Figure 2B). Directed by compound **S1** in the training set, the prenyl group was replaced by an alkyl group and removed to the C-7 position to change the molecule into a chain shape, termed the hydrophobic tail. The carbonyl and hydroxyl were replaced by a hydroxamic acid, which shares an approximate relative distance between the two groups. This part was designated as the hydrophilic head and served

as the H-bond donor and acceptor. Since the designed hydroxamic acid is one of the most prominent zinc binding groups (ZBGs) used in the design of metallohydrolase inhibitors, we did not introduce another negatively ionizable group, which has been discussed as a ZBG above.

This resulted in the design of the first series of inhibitors (**1a-1f**, Table 1). The initial compound **1a** contained a tail of C₄ alkyl group, sharing a similar length to the prenyl group of α -mangostin. As shown in Figure 2D, the benzene and hydrophobic tail of compound **1a** were mapped to the two HY features of Hypo 1, while its OH group mapped to HBD. The HBA and NI were missed. As most ASM inhibitors share a very long hydrophobic chain, we extended the length of the alkyl moiety to make it more suitable to the pharmacophore (**1b-1f**). As a result, compound **1b** with a C₈ hydrophobic chain exhibited a better mapping result than **1a**. The benzene and the 3rd carbon atom at the hydrophobic tail mapped with the two HY groups, while the hydroxamic acid head mapped well with the HBA and HBD features (Figure 2E).

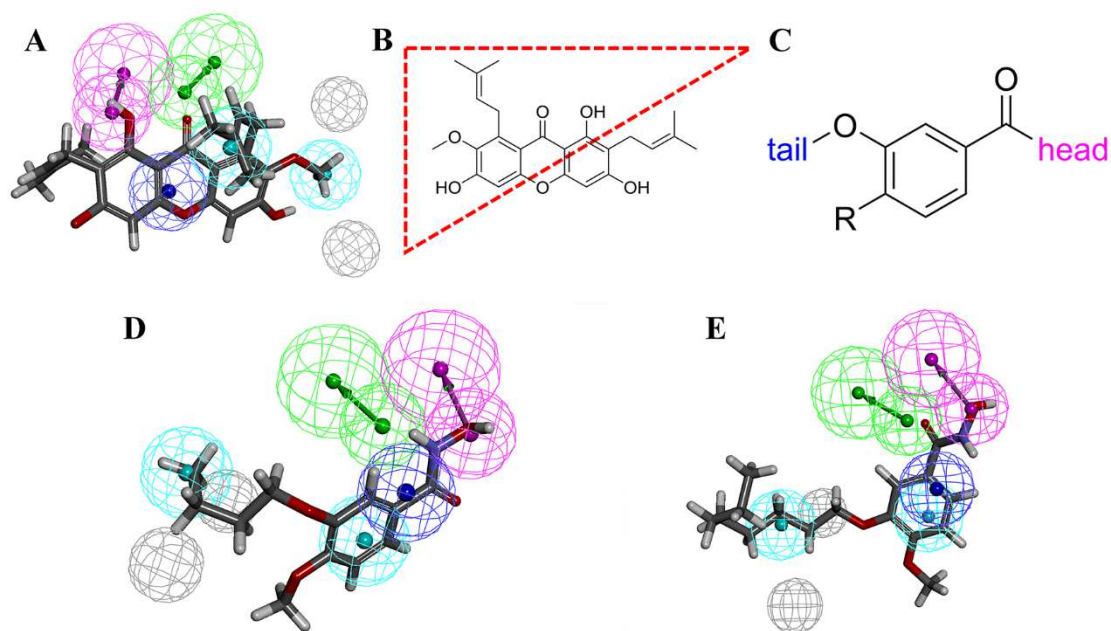


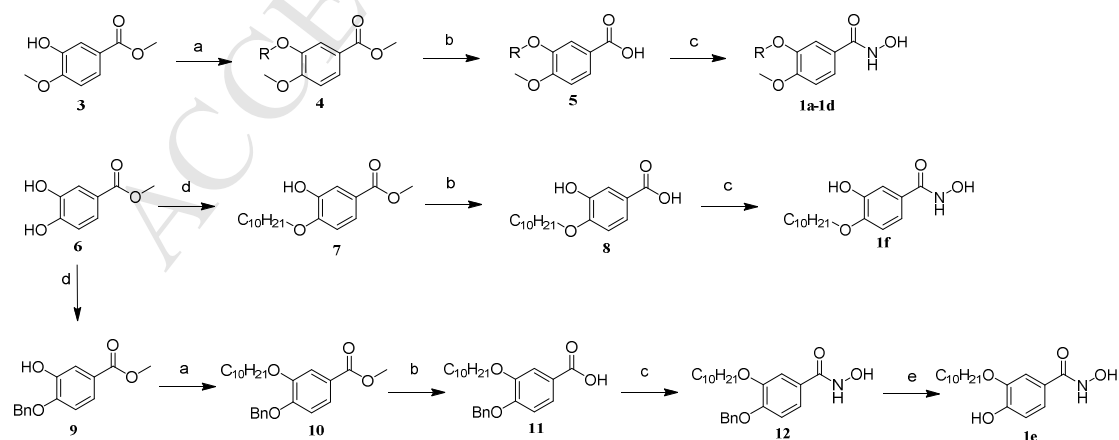
Figure 2. Pharmacophore based design of novel ASM inhibitors. (A) Mapping of Hypo 1 with α -mangostin. (B) The structure of α -mangostin. (C) General structure of the designed inhibitors. (D) Mapping of Hypo 1 with compound **1a**. (E) Mapping of Hypo 1 with compound **1b**. The color key is the same as defined in Figure 1.

Various modifications of series 1 were undertaken to develop a deeper understanding of structure–activity relationships (Table 2). We suspected that a flexible hydrophilic head carrying a carbonyl and a hydroxyl may be more suitable for

the HBA and HBD features in Hypo 1. To test this hypothesis, compounds **2a-2d** were prepared with good pharmacophore fit values from 5.34 to 6.87. As the methoxy group at C-4 of compound **2** seemed redundant in the mapping result of Hypo 1, we prepared compounds **2h-2j**, in which the methoxy was replaced by hydrogen. We next turned our attention to the hydrophobic tail. Introduction of more rigid groups to restrict the conformations may improve the activity. Thus, compounds **2k-2o** were designed. Mapping results showed that a benzyl substituent at C-3 of the molecule made it more suitable for the pharmacophore, such as **2k** and **2l** (Figure S2). The carbonyl and hydroxyl from the hydrophilic head mapped with the HBA and HBD, respectively, while the two benzene rings mapped well with the two HY groups.

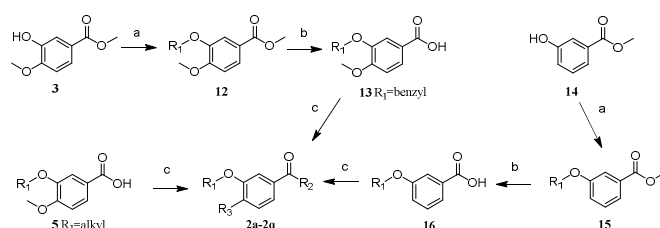
Synthesis of title compounds

We began the synthesis from two commercially available materials **3** and **6**. As depicted in Scheme 1, compounds **4** were obtained by substitution with suitable alkyl bromides in the presence of K_2CO_3 and KI, while compounds **7** and **9** were selectively prepared from substrate **6** since the benzoate activated the hydroxyl at C-4. Compound **9** was further substituted with 1-bromodecane to afford **10**. Products **4**, **7**, and **10** were allowed to hydrolyze to give the key intermediate **5**, **8**, and **11**, respectively. In the last step, the carboxylic acid intermediates were activated by thionyl chloride and were converted to the hydroxamic acid (**1a-1d**, **12**, **1g**) by adding them to a solution of hydroxylamine base. The solution was freshly prepared from hydroxylamine hydrochloride with NaOH in tetrahydrofuran and water. Compound **1e** were prepared by debenzoylation of **13** catalyzed by Pd/C under a hydrogen atmosphere.



Scheme 1. Reagents and conditions:(a) RBr, K₂CO₃, KI, acetone, 60 °C; (b) NaOH, MeOH, H₂O, 100 °C; (c) i: SOCl₂, DMF, CH₂Cl₂, ii: hydroxylamine hydrochloride, NaOH, THF, H₂O, rt; (d) BnBr, K₂CO₃, acetone, 60 °C; (e) Pd/H₂, MeOH, rt.

Compounds **2h-2p** in the second series were prepared according to the similar procedure described above, as illustrated in Scheme 2. The key intermediates **5**, **14**, and **17** were converted to various amides in the presence of 4-dimethylaminopyridine and 1-ethyl-3-(3-dimethylaminopropyl) carbodiimide hydrochloride in anhydrous DMF, yielding **2a-2g**, and **2q** (Scheme 2).



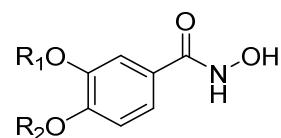
Scheme 2. Reagents and conditions: (a) RBr, K₂CO₃, KI, acetone, 60 °C; (b) NaOH, MeOH, H₂O, 100 °C; (c) EDCI, DMAP, CH₂Cl₂, rt, or i: SOCl₂, DMF, CH₂Cl₂, ii: hydroxylamine hydrochloride, NaOH, THF, H₂O, rt.

Biological screening and structure–activity relationship studies of the ASM inhibitors

Enzymatic assays of the target compounds were performed *in vitro* to confirm the results predicted by the pharmacophore model (Table 1 and Table 2). Compound **1a** with two features missing did not showed any inhibitory activity. However, when the lipid tail was lengthened, compounds **1b-1d** showed more potent activity than the lead compound, α -mangostin. Compound **1c** was found most active (0.48 μ M) among these molecules, about 50-fold more potent than α -mangostin (24.74 μ M), indicating that the hydrophobic tail with a length of C₁₀ was most feasible. Compound **1e** was less potent than compound **1c**, indicating that the free hydroxyl at the C-4 position had a negative effect on the activity. A certain angle between the tail and head is needed in the molecule as we found compound **1f** with the tail at C-4 position showed loss of activity. Corresponding carboxylic intermediates of the title compounds were also tested for their inhibitory activity on ASM. However, none of these intermediates was active, indicating that the binding mode of Zn²⁺ was not due to the effects of anion. On the whole, 4 out of the 6 designed compounds showed more potent activity than the lead compound, showing a high hit ratio. Taking into account the mapping

results, we can conclude that at least four features are essential to produce the most active compounds.

Table 1. The structures of series 1, pharmacophore mapping values and observed activities.



No.	R ₁	R ₂	Predicted IC ₅₀ (μM)	Fit value	Observed IC ₅₀ (μM)
1a	C ₄ H ₉	Me	18.69	5.34	-
1b	C ₈ H ₁₇	Me	13.89	5.41	16.09 ± 1.23
1c	C ₁₀ H ₂₁	Me	13.58	5.41	0.48 ± 0.10
1d	C ₁₂ H ₂₅	Me	13.56	5.42	18.55 ± 2.34
1e	C ₁₀ H ₂₁	H	0.91	6.59	17.43 ± 0.98
1f	H	C ₁₀ H ₂₁	19.1	5.27	-
α-M^a	-	-	20.06	5.25	24.74 ± 6.01

^a**α-M:** α-mangostin. Data are expressed as means ± SD of 3 experiments.

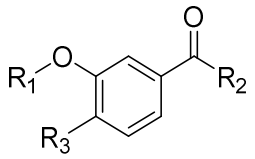
As to series 2, none of the compounds **2a-2d** were more effective inhibitors of ASM. Additionally, compounds **2f** and **2g** lacking a H-bond donor and **2e** with esterification of the hydroxamic acid were synthesized for comparison. As expected, these changes resulted in disappearance of activity of such compounds (Table 2). From the above result, we rationalized that the hydroxamic acid was an essential group for the inhibitory activity. This outcome may be attributed to its strong chelation of the Zn²⁺ in the catalytic center of ASM.

Compound **2i** (1.42 μM) was found to be 17-fold more potent than the lead compound, although it showed less activity than **1c**. This result indicated the C-4 methoxy group may be an important factor for the activity. Similarly, compound **2k** (10.49 μM) was found to be 2-fold more potent than α-mangostin, while **2l** showed a great decrease of activity (60.42 μM). Although the two compounds shared a similar fit value, they showed differences in the pharmacophore mapping mode and the observed activity. We suspected that restriction by the C-4 methoxy group of **2k** reduced the entropic penalty for achieving the desired transition state and led it to maintain the preferential conformation to inhibit the enzyme. The same phenomenon can also be found between compound **2o** and **2p**. However, this observation needs

further verification since compounds **2h** and **2g** showed comparable activity to that of compounds **1b** and **1d**, respectively.

In addition, the hydrophobic benzyl tail of **2k** shared a similar length (4.971 Å, predicted by Chem 3D) to that of the inactive compound **1a** (4.927 Å), demonstrating that a rigid tail was much more effective than the flexible alkyl. Compound **2k** was less potent than **1c** and **2i**. A probable reason is the benzyl tail was much shorter than the C₁₀ length of **1c**. When the benzyl was substituted by either nitrile or methoxy groups, compounds **2m** and **2n** showed a decrease of activity. In contrast, a hydrophobic bromine substituent increased the inhibitory activity, like compound **2o** and **2p**, as compared with **2k** and **2l**, respectively. This result may be caused by the N or O atom affecting the hydrophobicity of the tail. The absence of activity in compound **2q** came as no surprise, since it shared a much less effective head like **2a** or **2c**. From the above results, we can conclude that a hydrophobic tail with appropriate length and rigidity was very favorable for the inhibitory activity.

Table 2. Structure, pharmacophore mapping and observed activities of series 2 compounds.



No.	R ₁	R ₂	R ₃	Predicted IC ₅₀ (μM)	Fit value	Observed IC ₅₀ (μM)
2a	C ₁₀ H ₂₁	NH(CH ₂) ₂ OH	OMe	0.48	6.87	71.00 ± 9.34
2b	C ₁₀ H ₂₁	NHCH ₂ CH(OH)CH ₃	OMe	16.19	5.34	85.20 ± 9.49
2c	C ₈ H ₁₇	NH(CH ₂) ₂ OH	OMe	14.60	5.4	-
2d	C ₈ H ₁₇	NHCH ₂ CH(OH)CH ₃	OMe	15.17	5.37	-
2e	C ₁₀ H ₂₁	NHOMe	OMe	-	-	-
2f	C ₁₀ H ₂₁	2-aminopyridine	OMe	-	-	-
2g	C ₈ H ₁₇	2-aminopyridine	OMe	-	-	-
2h	C ₈ H ₁₇	NHOH	H	0.69	6.71	17.42 ± 1.45
2i	C ₁₀ H ₂₁	NHOH	H	0.63	6.75	1.42 ± 0.112
2j	C ₁₂ H ₂₅	NHOH	H	14.76	5.38	13.06 ± 2.32
2k	Benzyl	NHOH	OMe	0.57	6.80	10.49 ± 0.87
2l	Benzyl	NHOH	H	0.77	6.66	60.42 ± 4.67
2m	4-Cyanobenzyl	NHOH	H	35.87	5.00	52.87 ± 4.60
2n	4-methylbenzyl	NHOH	H	26.15	5.13	42.68 ± 5.26

2o	4-Bromobenzyl	NHOH	OMe	1.38	6.41	7.78 ± 0.81
2p	4-Bromobenzyl	NHOH	H	1.88	6.28	19.42 ± 1.51
2q	Benzyl	NH(CH ₂) ₂ OH	OMe	17.90	5.29	-

Data are expressed as means ± SD of 3 experiments.

Compound **1c** and **2i** were also tested their inhibitory potency towards neutral sphingomyelinase (NSM). As a result, none of the two compounds inhibited NSM at 100 μM (Figure S5), suggesting very high selectivity of **1c** and **2i**. In addition, we aimed to discover ASM inhibitors that functioned in direct manners, therefore the Lineweaver-Burk plots were used for further confirmation about competitive/non-competitive inhibition of ASM by compound **1c**. As shown in Figure 3, compound **1c** displayed competitive inhibition against ASM.

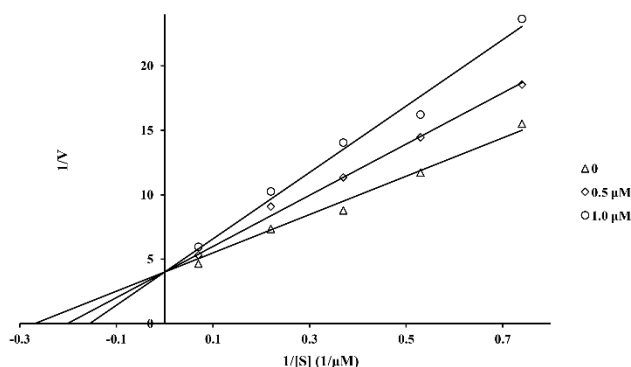


Figure 3. Lineweaver-Burk plots of acid sphingomyelinase activity over a range of substrate (NBD-SM) concentrations in the absence and presence of **1c** at concentrations 0.5 μM, 1.0 μM, and 5 μM (ASM was almost completely inhibited at 5 μM and the data are beyond this figure). The data are representative of triplicate experiments.

Ceramide generation inhibition assay

In order to explore the intracellular potency of the inhibitor to block Cers production, compound **1c** was selected to measure inhibition of the generation of Cers. The NIH3T3 cell line was cultivated and treated with different concentrations of **1c**, then the amount of Cers and SM was evaluated by the LC-MS-MS technology. As shown in Figure 4, upon treatment with **1c** (5 μM, 10 μM, and 20 μM), the total amount of Cers was significantly decreased in a dose dependent manner (26.1 %, 37.0 %, 42.6 %, respectively); while the total amount of SM was increased (31.9 %, 36.4 %, 37.5 %, respectively). Besides, compound **1c** showed much better IC₅₀ value (0.48 μM) in the NBD assay. One possible reason is that the NBD assay was performed directly on proteins, while the ceramide determination was performed on live cells.

Membrane permeability of **1c** and the complex metabolic environment of cells may affect the activity. Moreover, because of the introduction of NBD group, the NBD-sphingomyelin might have a little lower affinity compared to natural sphingomyelin. Since **1c** is a competitive inhibitor, it might exhibit better IC₅₀ data in the NBD assay. This result confirmed that compound **1c** is an effective ASM inhibitor in the cell environment.

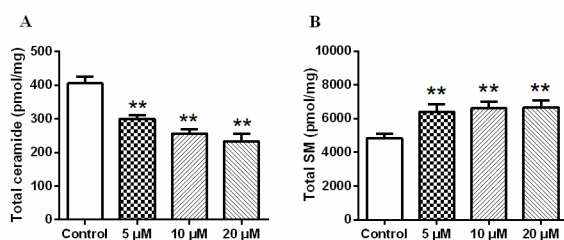


Figure 4. Compound **1c** inhibited the generation of Cers. Human NIH3T3 cells were treated with **1c** at the doses of 0 μM (Control), 5 μM, 10 μM, and 20 μM. (A) The amount of total Cers. (B) The amount of total sphingomyelin (SM). Values are mean ± SD from three independent experiments, Student's t-test **P < 0.01 compared to control group.

Characterization of compound **1c** as potent anti-apoptosis and anti-inflammation agents

Significantly increased levels of Cers in pathological tissues has the ability to induce apoptosis. Thus, compound **1c** was tested in an anti-apoptosis study to determine its protective effects on cell. As shown in Figure 5, treatment with compound **1c** effectively increased cell viability even at the low concentration of 10 μM. The apoptosis prevention function of **1c** at a lower concentration was more effective than the above ceramide inhibition activity. It is reasoned that the ceramide inhibition assay was performed on normal cells, in which ASM is not highly expressed. While UV induced great increase of the activity of ASM in the apoptosis assay. Thus, the effect of **1c** on apoptotic cells may be more obvious.

However, there was no concentration dependency. Toxicity test of **1c** on NIH3T3 cells by MTT assay found an IC₅₀ value of 51.38 ± 3.94 μM (Table S1). This result may rationalize the phenomenon that higher concentration of **1c** didn't show higher anti-apoptosis activity.

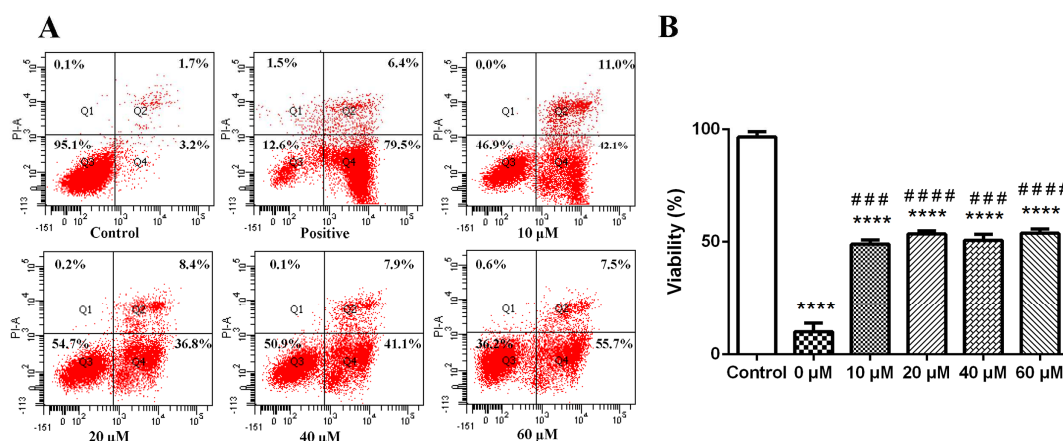


Figure 5. Survival of human NIH3T3 cells upon exposure to UV in the presence of **1c**. Cells were treated with **1c** (from 0 μ M to 60 μ M) for 20 h, followed by irradiation with UV light (315 nm) for 5 min. The cells were then maintained for another 24 h. The apoptosis status of the cells was measured by flow cytometry. (A) Flow cytometry data (full data are shown in supplementary material). (B) Cell viability as determined by percentage of Q3 region. Values are expressed as mean \pm SD from three independent experiments, **** p <0.0001 compared to control group, ### p <0.001 compared to 0 μ M group, #### p <0.0001 compared to 0 μ M group.

Next, whether ASM inhibitor **1c** can effectively prevent the increase of UV-induced ceramide production in the apoptosis assay was further explored. Amitriptyline was selected as a positive control since it has been shown to functional inhibit ASM and decrease cellular Cers content [19]. Initially, one out of the four repeated experiments was used to determine the viability of cells. Results confirmed that both amitriptyline and **1c** exhibited dose dependent cytoprotection (Figure S7). Then changes of the ceramide content of the rest samples were investigated by LC-MS-MS technology. Figure 6 obviously revealed the statistical results that UV treatment induced a notable increase of Cers (about 200 %), a phenomenon that was consistent with the previous reports [42, 43]. It is noteworthy that amitriptyline and **1c** could dose dependently inhibit this change. Furthermore, **1c** with a concentration of 50 μ M restored Cers to a normal level (105.777 pmol/mg), comparing to the control group (107.686 pmol/mg). This result further validated that the mechanism by which compound **1c** protected cells from apoptosis was to reduce the content of ceramide by inhibiting ASM.

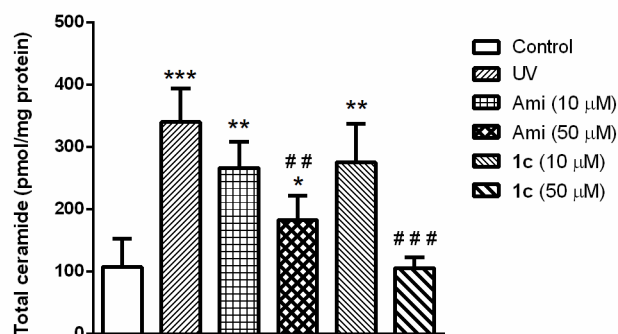


Figure 6. UV induced an increase of Cers, while compound **1c** could block this phenomenon. Ami, amitriptyline. Values are expressed as mean \pm SD from three independent experiments, ** $p < 0.01$ compared to control group, # # $p < 0.01$ compared to UV group, # $p < 0.05$ compared to UV group.

Additionally, ASM-Cers-related cell inflammation has been found to be involved in several inflammatory diseases, such as atherosclerosis [44], cystic fibrosis [45], and other lung diseases [1]. Here, compound **1c** was selected to investigate the inhibitory effects of IL-6, IL-8 production in LPS-induced NIH3T3 cells. As shown in Figure 7, LPS induced a robust increase in transcription of IL-6 and IL-8. Treatment with compound **1c** significantly reduced the upregulated cytokine in a dose-dependent manner, although it did not show a significant effect at the concentration of 2.5 μM in the IL-8 assay. These data suggest that direct inhibition of ASM can reduce the pathological inflammatory response.

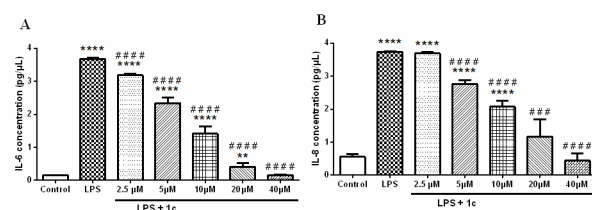


Figure 7. Acid sphingomyelinase inhibitor **1c** reduces inflammation in cells. Normal NIH3T3 cells were induced by LPS and then treated with different concentrations of **1c**. Cytokines were evaluated by ELISA. ** $p < 0.01$ compared to control group, **** $p < 0.0001$ compared to control group, # # $p < 0.001$ compared to LPS group, # # # $p < 0.0001$ compared to LPS group.

Molecular docking

The crystal structure (PDB code: 5fi9) of ASM was resolved recently and investigations showed that its catalytic domain adopts a calcineurin-like fold with two zinc ions. Furthermore, two key residues His 280 and His 317 are essential for Cers to

leave [38]. Comparison of the pharmacophore and the X-ray structure revealed some consistent features. The catalytic center of ASM, which is consist of ions and polar amino acids such as His and Asp, may be the potential corresponding site of the HBD, NI, and HBA features of the pharmacophore. A hydrophobic shallow groove of the protein also satisfies the HY groups of the pharmacophore (Figure S8). To validate this assumption and illustrate the potential binding modes between the inhibitors and the enzyme, docking simulations of compounds **1a**, **1c**, and **2e** were performed in the binding pocket of ASM using the CCDC Gold Suite 5.3.0 software.

Compound **1c** (green) exhibited a similar binding mode with 1-aminodecylidene bis-phosphonic acid (AbPA) (blue), a ligand co-crystallized with ASM (Figure 8A). The hydroxamic acid group was inserted into the innermost binding sites of the active pocket while the lipid tail stretched into a shallow groove. The carbonyl group at the head formed one hydrogen bond with residue Asp 276. This group was found to coordinate with one zinc. The hydroxyl at the head formed three hydrogen bonds with the residues His 206 and His 280 and was found to coordinate with the second zinc. Meanwhile, Pi conjugation was found between the benzene ring of **1c** and His 455 (Figure 8B).

It is worth noting that shortening the tail (**1a**) or esterification of the head (**2e**) led to a remarkable loss of the potency. This finding was also supported by the docking studies. The head group of **1a** matched the catalytic center, but its tail was too short to fill the groove. In contrast, **2e** maintained a suitable tail, while its head deviated far from the catalytic center (Figure S9).

In conclusion, the docking results clearly indicated that the hydroxamic acid group was critical for the inhibitors to bind to the protein and to effect inhibitory potency, which was consistent with the SAR analyses. These results provide great assistance for the rational design of new ASM inhibitors that will better exploit the shape of the active site.

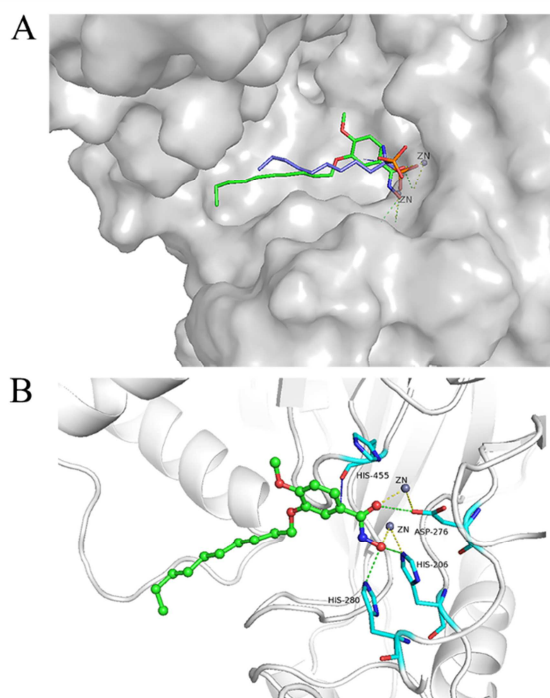


Figure 8. The binding modes of **1c** with ASM. (A) Superposition of **1c** and the original bisphosphonate ligand in the crystal. (B) Binding mode of the active inhibitors. Green: **1c**; blue: AbPA. Hydrogen bonds are shown as green lines, metal contact in yellow, and Pi contact in blue.

Conclusions

In the present study, we generated an excellent ligand-based pharmacophore model using a series of known ASM inhibitors. The model showed good statistical parameters in its validation process and was used to perform the simplification and optimization of the lead compound, α -mangostin. Enzymatic assays found that four out of the six compounds in series 1 showed greater potency than α -mangostin, indicating the pharmacophore model was highly effective. Further mapping-guided optimization together with empirically-based structural modifications provided a detailed structure-activity relationship investigation, which identified compound **1c** as the most active and selective ASM inhibitor. Treatment by **1c** on the NIH3T3 cell line efficiently decreased the total amount of Cers generation in a dose-dependent manner. Significantly, **1c** exhibited very excellent *in vitro* results against apoptosis and inflammation, two events that are typical in the pathological process of Cers-associated diseases. MTT assay indicated a much higher cytotoxic IC_{50} ($51.38 \mu M$) than its inhibitory activity ($0.48 \mu M$). In the apoptosis assay, Cers was found significant increased under irradiation of UV, while amitriptyline or **1c** treatment

could attenuate this change and protected cells from UV induced apoptosis. Docking simulations directly provided detailed information about binding between **1c** and ASM. Taken together, the pharmacophore model and the SAR analyses make new and significant contributions toward understanding ASM inhibition. The information gained here offers practical guidance in the search for novel lead compounds that will be more potent ASM inhibitors. Furthermore, the promising compounds described here may serve as valuable pharmacological tools, which can be applied to verify the role of ASM as a potential drug target in various ceramide-associated diseases.

Experimental Section

Pharmacophore modelling

Biological activity data represented as IC_{50} (μM) were obtained from literature and the PubChem BioAssay data in NCBI. Chemical structures of selected ASM inhibitors were separated into training and test sets on the basis of activity and structural diversity (Supplementary Table S1 and S4, respectively). The training set compounds were used to generate pharmacophore models using the 3D QSAR Pharmacophore Generation protocol of DS 3.0. Four features were selected as the most found features viz. hydrogen bond acceptor (HBA), hydrogen bond donor (HBD), hydrophobic (HY) and negatively ionizable (NI). The conformation generation was chosen as “best”, which ensures the best coverage of conformational space. The uncertainty value was defined as 2, representing the ratio of the uncertainty range of the measured activity against the actual activity for each compound. Other settings were kept the default. In the protocol run, ten pharmacophore hypotheses were generated on the basis of a high correlation coefficient (r), low total cost, and low RMSD. Further quality assessment and validation of the pharmacophore model was done using the test set compounds in DS 3.0.

Molecular docking

The docking study was performed with CCDC GOLD 5.3.0 software (Cambridge, UK). The co-crystal structures of ASM with an inhibitor (AbPA) (PDB code: 5fi9) was chosen as the receptor.³⁴ Small molecules were drawn in ChemDraw and the initial lowest energy conformations were calculated in Chem3D. Protein was preliminary prepared in DS 3.0 with adding hydrogens, deleting glycosyls and water and conducting the “Clean Protein” protocol. The prepared protein was then imported

into GOLD and edited with extracting ligand. The binding site was defined at the position of the original included ligand AbPA. Goldscore_P450_csd was chosen as the configuration template and GoldScore was chosen as scoring function. Other parameters kept default. Docking poses were loaded into Gold software for a visualization of ligand-receptor interactions and analysis.

Chemistry

General: Starting materials and reagents were obtained from commercially available sources with high-grade purity. Thin-layer chromatography (TLC) was performed on Merck silica gel plates (Merck silica gel plates GF254, Germany) and visualized under UV light (254 nm). Column chromatography was performed with Merck Kieselgel 60 (200-300 mesh, Germany). Melting points were determined on a MEL-TEMP II apparatus (Laboratory Devices, MA, USA). ¹H NMR and ¹³C NMR spectra were recorded on a Bruker AV-300 MHz instrument (Bruker Biospin AG, Switzerland) in CDCl₃ or DMSO-d₆ with TMS as the internal standard. MS were obtained on Waters Q-ToF microTM (Waters, MA, USA) with the ESI (+, -) protonation interface. High-resolution mass spectra (HRMS) were recorded on Q-ToF Premier hybrid mass spectrometer with electron spray ionization (ESI). HPLC analysis was performed on a Shimadzu SPD-20A/20AV HPLC system (Shimadzu, Tokyo, Japan). The column used was a C18 column (5 μm micron, 250 × 4.60 mm) at a temperature of 30 °C and a flow rate of 1.0 mL/min. The purity of title compounds was higher than 95%, which was assessed at 254 nM under a condition of methanol /water (0.1% AcOH) (a ratio of 65:35 for **1a**, **1e**, **2k-2q**; a ratio of 90:10 for **1b-1d**, **1f**, **2a-2j**). NBD-Cers were determined at 525 nM under a condition of methanol (0.1% TFA) /water (89:11). NBD-SM was purchased from Avanti (AL, USA). All title compounds were examined for PAINS and passed. Anhydrous reactions were carried out in dried glassware under a nitrogen atmosphere. The boiling range for petroleum ether was 60–90 °C. Key intermediates were synthesized followed the common used methods in literatures.

General procedure for the Preparation of compounds **1a-1d**, **13**, **1f** and **2h-2p**

A mixture of the substrate (100 mg), dimethyl formamide (1 drop) and thionyl chloride (3 equiv.) in anhydrous dichloromethane (10 mL) was heated to reflux for 3 h and concentrated to remove the thionyl chloride and solvent. The concentrate was then redissolved by anhydrous tetrahydrofuran (10 mL) and slowly added into a

solution of hydroxylamine, which was freshly prepared by dissolving hydroxylammonium chloride (5 equiv.) and NaOH (5 equiv.) into tetrahydrofuran (4 mL) and water (0.5 mL). After the drop add, the mixture was stirred at room temperature for 5 min, concentrated in vacuum and purified by chromatography on silica gel to afford the title product.

3-Butoxy-N-hydroxy-4-methoxybenzamide (1a)

White solid (72 mg, 68.4 %), M.P. 149-150 °C, ¹H-NMR (300 MHz, DMSO-d₆): δ 11.06 (s, 2H), , 8.90 (s, 2H), 7.38-7.35 (m, 2H), 7.01-6.98 (m, 1H), 4.00 (t, *J* = 6.30 Hz, 2H), 3.80 (s, 3H), 1.75-1.66 (m, 2H), 1.50-1.43 (m, 2H), 0.96 (t, *J* = 7.20 Hz, 3H); ¹³C NMR (75 MHz, DMSO-d₆): δ 164.42, 151.84, 148.12, 125.36, 120.50, 111.78, 111.69, 68.39, 56.07, 31.24, 19.20, 14.14; HRMS (ESI-TOF): calcd for C₁₂H₁₈NO₄ [M + H]⁺ 240.1230, found 240.1233.

N-Hydroxy-4-methoxy-3-(octyloxy)benzamide (1b)

White solid (63 mg, 60 %), M.P. 168-171 °C, ¹H-NMR (300 MHz, DMSO-d₆): δ 11.06 (s, 1H), 8.89 (s, 1H), 7.38-7.34 (m, 2H), 7.01-6.98 (m, 1H), 3.99 (t, *J* = 6.60 Hz, 2H), 3.79 (s, 3H), 1.74-1.67 (m, 2H), 1.41-1.39 (m, 2H), 1.27 (m, 8H), 0.87-0.84 (m, 3H); ¹³C NMR (75 MHz, DMSO-d₆): δ 164.41, 151.85, 148.12, 125.37, 120.49, 111.81, 111.71, 68.72, 56.08, 31.70, 29.17, 29.15, 29.13, 25.97, 22.54, 14.41; HRMS (ESI-TOF): calcd for C₁₆H₂₆NO₄ [M + H]⁺ 296.1856, found 296.1860.

3-(Decyloxy)-N-hydroxy-4-methoxybenzamide (1c)

White solid (71 mg, 67.7 %), M.P. 118-120 °C, ¹H-NMR (300 MHz, DMSO-d₆): δ 11.04 (s, 1H) , 8.87 (s, 1H), 7.38-7.36 (m, 2H), 7.01-6.98 (m, 1H), 3.99 (t, *J* = 6.30 Hz, 2H), 3.80 (s, 3H), 1.74-1.70 (m, 2H), 1.41-1.39 (m, 2H), 1.26 (m, 12H), 0.86-0.84 (m, 3H); ¹³C NMR (75 MHz, DMSO-d₆): δ 164.44, 151.87, 148.14, 125.38, 120.50, 111.86, 111.72, 68.94, 56.08, 31.76, 29.48, 29.42, 29.22, 29.15, 25.97, 22.54, 14.39; HRMS (ESI-TOF): calcd for C₁₈H₃₀NO₄ [M + H]⁺ 324.2169, found 324.2174.

3-(Dodecyloxy)-N-hydroxy-4-methoxybenzamide (1d)

White solid (78 mg, 74.7 %), M.P. 128-129 °C, ¹H-NMR (300 MHz, DMSO-d₆): δ 11.05 (s, 1H), 8.88 (s, 1H), 7.36 (m, 2H), 7.00 (m, 1H), 3.97 (m, 2H), 3.80 (s, 3H), 1.72 (m, 2H), 1.25 (m, 18H), 0.86 (m, 3H); ¹³C NMR (75 MHz, DMSO-d₆): δ 164.04, 151.88, 148.15, 125.39, 111.88, 111.74, 68.74, 56.08, 31.76, 29.48, 29.17, 25.97, 22.54, 14.37; HRMS (ESI-TOF): calcd for C₂₀H₃₄NO₄ [M + H]⁺ 352.2482, found 352.2482

4-(Benzyloxy)-3-(decyloxy)-N-hydroxybenzamide (13)

White solid (57 mg, 54.9 %), ¹H-NMR (300 MHz, CDCl₃): δ 7.44-7.31 (m, 6H), 7.20 (m, 1H), 6.89 (m, 1H), 5.18 (s, 2H), 4.05 (m, 2H), 1.84 (m, 2H), 1.47 (m, 2H), 1.27 (m, 12H), 0.90 (t, *J* = 6.00 Hz, 3H); ESI-MS *m/z*: 422 [M + Na]⁺.

4-(Decyloxy)-N,3-dihydroxybenzamide (1f)

White solid (56 mg, 53.3 %), M.P. 128-130 °C, ¹H-NMR (300 MHz, DMSO-d₆): δ 11.45 (s, 1H), 9.21 (s, 1H), 7.40-7.35 (m, 2H), 6.97-6.95 (m, 1H), 4.02 (t, *J* = 6.30 Hz, 2H), 1.74-1.70 (m, 2H), 1.41-1.39 (m, 2H), 1.25 (m, 12H), 0.88 (t, *J* = 6.30 Hz, 3H); ¹³C NMR (75 MHz, DMSO-d₆): δ 167.63, 151.42, 146.70, 123.39, 122.02, 116.57, 112.72, 68.64, 31.75, 29.48, 29.42, 29.25, 29.16, 29.09, 25.88, 22.55, 14.40; ESI-MS *m/z*: 332 [M + Na]⁺.

N-Hydroxy-3-(octyloxy)benzamide (2h)

White solid (73 mg, 68.9 %), M.P. 85-87 °C, ¹H-NMR (300 MHz, DMSO-d₆): δ 11.18 (s, 1H), 9.01 (s, 1H), 7.34-7.29 (m, 3H), 7.06-7.04 (m, 1H), 4.01 (t, *J* = 6.3 Hz, 2H), 1.74-1.69 (m, 2H), 1.41 (m, 2H), 1.26 (m, 8H), 0.86-0.38 (m, 3H); ¹³C NMR (75 MHz, DMSO-d₆): δ 164.37, 159.03, 134.58, 129.94, 119.43, 117.86, 113.02, 68.05, 31.69, 29.19, 29.12, 29.09, 25.96, 22.54, 14.48; HRMS (ESI-TOF): calcd for C₁₅H₂₄NO₃ [M + H]⁺ 266.1751, found 266.1747.

3-(Decyloxy)-N-hydroxybenzamide (2i)

White solid (82 mg, 77.8 %), M.P. 107-108 °C, ¹H-NMR (300 MHz, DMSO-d₆): δ 11.16 (s, 1H), 9.01 (s, 1H), 7.38-7.29 (m, 3H), 7.07-7.03 (m, 1H), 4.01 (t, *J* = 6.30 Hz, 2H), 1.74-1.69 (m, 2H), 1.41-1.37 (m, 2H), 1.25 (m, 12H), 0.88 (t, *J* = 6.30 Hz, 3H); ¹³C NMR (75 MHz, DMSO-d₆): δ 164.34, 159.03, 134.57, 129.93, 119.42, 117.85, 113.01, 68.04, 31.75, 29.47, 29.41, 29.22, 29.15, 29.09, 25.95, 22.54, 14.38; HRMS (ESI-TOF): calcd for C₁₇H₂₈NO₃ [M + H]⁺ 294.2064, found 294.2067.

3-(Dodecyloxy)-N-hydroxybenzamide (2j)

White solid (76 mg, 72.4 %), M.P. 115-117 °C, ¹H-NMR (300 MHz, DMSO-d₆): δ 11.18 (s, 1H), 9.02 (s, 1H), 7.36-7.29 (m, 2H), 7.06-7.04 (m, 1H), 4.00 (t, *J* = 6.60 Hz, 2H), 1.73-1.69 (m, 2H), 1.41 (m, 2H), 1.24 (m, 16H), 0.85-0.83 (m, 3H); ¹³C NMR (75 MHz, DMSO-d₆): δ 164.34, 159.03, 134.57, 129.93, 119.42, 117.85, 112.99, 68.03, 31.76, 29.48, 29.24, 29.18, 29.10, 25.96, 22.56, 14.39; HRMS (ESI-TOF): calcd for C₁₉H₃₂NO₃ [M + H]⁺ 322.2377, found 322.2384.

3-(Benzyloxy)-N-hydroxy-4-methoxybenzamide (2k)

White solid (86 mg, 81.3 %), M.P. 178-179 °C, ¹H-NMR (300 MHz, DMSO-d₆): δ 11.06 (s, 1H), 8.90 (s, 1H), 7.47-7.34 (m, 7H), 7.34-7.02 (m, 1H), 5.12 (s, 2H), 3.82 (s, 3H); ¹³C NMR (75 MHz, DMSO-d₆): δ 164.37, 152.03, 147.79, 137.39, 128.87, 128.34, 128.26, 125.39, 120.88, 112.59, 111.85, 70.48, 56.16; HRMS (ESI-TOF): calcd for C₁₇H₁₆NO₄ [M + H]⁺ 274.1074, found 274.1079.

3-(Benzyloxy)-N-hydroxybenzamide (2l)

White solid (70 mg, 65.7 %), M.P. 174-176 °C, ¹H-NMR (300 MHz, DMSO-d₆): δ 11.22 (s, 1H), 9.06 (s, 1H), 7.48-7.31 (m, 8H), 7.18-7.14 (m, 1H), 5.15 (s, 2H); ¹³C NMR (75 MHz, DMSO-d₆): δ 164.33, 158.71, 137.32, 134.66, 130.03, 128.92, 128.35, 128.15, 119.77, 118.19, 113.55, 69.81; HRMS (ESI-TOF): calcd for C₁₄H₁₄NO₃ [M + H]⁺ 244.0968, found 244.0969.

3-((4-Cyanobenzyl)oxy)-N-hydroxybenzamide (2m)

White solid (75 mg, 70.8 %), M.P. 160-162 °C, ¹H-NMR (300 MHz, DMSO-d₆): δ 11.21 (s, 1H), 9.05 (s, 1H), 7.89-7.86 (m, 2H), 7.67-7.64 (m, 2H), 7.41-7.37 (m, 3H), 7.19-7.15 (m, 1H), 5.27 (s, 2H); ¹³C NMR (75 MHz, DMSO-d₆): δ 164.21, 158.36, 143.16, 134.73, 132.90, 130.12, 128.51, 120.04, 119.20, 118.21, 113.58, 111.00, 68.85; HRMS (ESI-TOF): calcd for C₁₅H₁₃N₂O₃ [M + H]⁺ 269.0921, found 269.0923.

N-Hydroxy-3-((4-methoxybenzyl)oxy)benzamide (2n)

White solid (73 mg, 70.0 %), M.P. 170-172 °C, ¹H-NMR (300 MHz, DMSO-d₆): δ 11.20 (s, 1H), 9.04 (s, 1H), 7.40-7.34 (m, 5H), 7.16-7.13 (m, 1H), 6.97-6.94 (m, 2H), 5.06 (s, 2H), 3.76 (s, 3H); ¹³C NMR (75 MHz, DMSO-d₆): δ 164.34, 159.50, 158.76, 134.61, 129.97, 129.16, 119.19, 118.19, 114.30, 113.55, 69.60, 55.55; HRMS (ESI-TOF): calcd for C₁₅H₁₆NO₄ [M + H]⁺ 274.1074, found 274.1076.

N-Hydroxy-3-((4-methoxybenzyl)oxy)benzamide (2o)

White solid (90 mg, 85.8 %), M.P. 149-151 °C, ¹H-NMR (300 MHz, DMSO-d₆): δ 11.06 (s, 1H), 8.99 (s, 1H), 7.62-7.42 (m, 5H), 7.05-7.03 (m, 1H), 5.11 (m, 2H), 3.82 (s, 3H); ¹³C NMR (75 MHz, DMSO-d₆): δ 164.26, 151.99, 147.55, 136.88, 131.82, 130.31, 125.36, 121.46, 120.99, 112.63, 111.85, 69.65, 56.17; HRMS (ESI-TOF): calcd for C₁₅H₁₆NO₄ [M + H]⁺ 352.0185, found 352.0179.

N-Hydroxy-3-((4-methoxybenzyl)oxy)benzamide (2p)

White solid (86 mg, 72.3 %), M.P. 160-161 °C, ¹H-NMR (300 MHz, DMSO-d₆): δ 11.18 (s, 1H), 9.00 (s, 1H), 7.62-7.59 (m, 2H), 7.44-7.35 (m, 4H), 7.16-7.14 (m, 1H), 5.14 (s, 2H); ¹³C NMR (75 MHz, DMSO-d₆): δ 164.26, 158.51, 136.80, 134.66,

131.85, 130.24, 121.46, 119.88, 118.19, 113.58, 68.99; HRMS (ESI-TOF): calcd for $C_{15}H_{16}NO_4 [M + Na]^+$ 343.9897, found 343.9893.

General procedure for the preparation of compounds 2a - 2g, 2q

A mixture of the carboxylic acid substrate (100 mg), 1-Ethyl-3-(3-dimethylaminopropyl) carbodiimide hydrochloride (3 equiv.), 4-dimethylaminopyridine (0.5 equiv.) and amine (3 equiv.) in anhydrous DMF (5 mL) was stirred at room temperature for 6 h under nitrogen atmosphere. The mixture was diluted with ethyl acetate (20 mL), washed with water (15 mL \times 3) and dried over Na_2SO_4 , concentrated and purified by chromatography on silica gel to afford the target products.

3-(Decyloxy)-N-(2-hydroxyethyl)-4-methoxybenzamide (2a)

White solid (62 mg, 54.4 %), M.P. 98-99 °C, 1H -NMR (300 MHz, $CDCl_3$): δ 7.43 (s, 1H), 7.28 (s, 1H), 6.90-6.87 (m, 1H), 6.60-6.58 (m, 1H), 4.10 (t, $J = 7.05$ Hz, 2H), 3.93 (s, 3H), 3.86 (m, 2H), 3.65 (m, 2H), 1.90-1.85 (m, 2H), 1.76-1.71 (m, 4H), 1.47 (m, 2H), 1.28 (m, 8H), 0.92 (t, $J = 6.12$ Hz, 3H); ^{13}C NMR (75 MHz, $CDCl_3$): δ 168.37, 152.27, 148.57, 126.60, 119.51, 112.01, 110.62, 69.18, 62.46, 56.02, 42.96, 31.88, 29.54, 29.38, 29.30, 29.11, 25.93, 22.66, 14.10; HRMS (ESI-TOF): calcd for $C_{20}H_{34}NO_4 [M + H]^+$ 352.2482, found 352.2486.

3-(Decyloxy)-N-(2-hydroxypropyl)-4-methoxybenzamide (2b)

White solid (69 mg, 58.2 %), M.P. 89-91 °C, 1H -NMR (300 MHz, $CDCl_3$): δ 7.43 (s, 1H), 6.89-6.87 (m, 1H), 6.52 (s, 1H), 4.10 (t, $J = 6.69$ Hz, 2H), 3.93 (s, 3H), 3.68-3.65 (m, 1H), 3.34-3.31 (m, 1H), 1.90-1.83 (m, 4H), 1.49-1.45 (m, 2H), 1.29-1.27 (m, 13H), 0.92 (t, $J = 6.12$ Hz, 3H); ^{13}C NMR (75 MHz, $CDCl_3$): δ 168.20, 152.29, 148.62, 126.73, 119.44, 112.15, 110.69, 69.21, 67.65, 56.04, 47.57, 31.87, 29.53, 29.37, 29.29, 29.12, 25.92, 22.65, 21.04, 14.07; HRMS (ESI-TOF): calcd for $C_{21}H_{36}NO_4 [M + H]^+$ 366.2639, found 366.2643.

N-(2-Hydroxyethyl)-4-methoxy-3-(octyloxy)benzamide (2c)

White solid (79 mg, 68.5 %), M.P. 85-87 °C, 1H -NMR (300 MHz, $CDCl_3$): δ 7.39-7.29 (m, 2H), 6.98 (s, 1H), 6.80-6.77 (m, 1H), 4.01 (t, $J = 6.6$ Hz, 2H), 3.96 (s, 3H), 3.76 (m, 2H), 3.56 (m, 2H), 1.81-1.76 (m, 2H), 1.40 (m, 2H), 1.24 (m, 8H), 0.85 (m, 3H); ^{13}C NMR (75 MHz, $CDCl_3$): δ 168.29, 152.24, 148.52, 126.63, 119.70, 112.12, 110.68, 56.00, 42.98, 31.78, 29.32, 29.12, 25.92, 22.61, 14.05; HRMS (ESI-TOF): calcd for $C_{18}H_{30}NO_4 [M + H]^+$ 324.2169, found 324.2173.

N-(2-Hydroxypropyl)-4-methoxy-3-(octyloxy)benzamide (2d)

White solid (83 mg, 69.0 %), M.P. 109-111 °C, ¹H-NMR (300 MHz, CDCl₃): δ 7.42 (s, 1H), 7.34-7.29 (m, 1H), 6.85-6.82 (m, 2H), 4.06-4.01 (m, 3H), 3.65-3.60 (m, 1H), 3.30 (m, 2H), 1.86-1.81 (m, 2H), 1.45 (m, 2H), 1.29-1.22 (m, 11H), 0.89-0.87 (m, 3H); ¹³C NMR (75 MHz, CDCl₃): δ 168.19, 152.24, 148.46, 126.71, 119.57, 112.16, 110.67, 56.02, 47.61, 31.78, 29.32, 29.17, 25.92, 22.62, 21.01, 14.05; HRMS (ESI-TOF): calcd for C₁₉H₃₂NO₄ [M + H]⁺ 338.2326. found 338.2333.

3-(Decyloxy)-N,4-dimethoxybenzamide (2e)

White solid (80 mg, 73.1 %), M.P. 115-117 °C, ¹H-NMR (300 MHz, CDCl₃): δ 7.36 (s, 1H), 7.24 (m, 1H), 6.88-6.85 (m, 1H), 4.09 (t, *J* = 6.90 Hz, 2H), 3.92-3.90 (s, 6H), 1.90-1.85 (m, 2H), 1.47-1.43 (m, 2H), 1.28 (m, 12H), 0.90-0.87 (m, 3H); ¹³C NMR (75 MHz, CDCl₃): δ 166.49, 152.64, 148.74, 124.22, 119.66, 111.85, 110.70, 69.20, 64.56, 56.03, 31.88, 29.54, 29.37, 29.30, 29.08, 25.92, 22.66, 14.09; HRMS (ESI-TOF): calcd for C₁₉H₃₂NO₄ [M + H]⁺ 338.2326, found 338.2330.

3-(Decyloxy)-4-methoxy-N-(pyridin-2-yl)benzamide (2f)

White solid (104 mg, 83.4 %), M.P. 83-83 °C, ¹H-NMR (300 MHz, CDCl₃): δ 9.23 (s, 1H), 8.50 (d, *J* = 8.43 Hz, 1H), 8.29-8.28 (m, 1H), 7.87-7.82 (m, 1H), 7.59-7.57 (m, 2H), 7.15-7.10 (m, 1H), 6.97 (d, *J* = 8.88 Hz, 1H), 4.14 (t, *J* = 6.84 Hz, 2H), 3.95 (s, 3H), 1.94-1.85 (m, 2H), 1.49-1.44 (m, 2H), 1.32 (m, 12H), 0.91 (t, *J* = 5.82 Hz, 3H); ¹³C NMR (75 MHz, CDCl₃): δ 165.40, 152.84, 151.78, 148.75, 147.41, 138.71, 126.52, 120.13, 119.67, 114.32, 111.96, 110.72, 69.20, 56.08, 31.89, 29.54, 29.37, 29.30, 29.09, 25.92, 22.66, 14.10; HRMS (ESI-TOF): calcd for C₂₃H₃₃N₂O₃ [M + H]⁺ 385.2486, found 385.2494.

3-(Decyloxy)-4-methoxy-N-(pyridin-3-yl)benzamide (2g)

White solid (108 mg, 84.9 %), M.P. 70-73 °C, ¹H-NMR (300 MHz, CDCl₃): δ 9.27 (s, 1H), 8.48-8.45 (m, 1H), 8.26-8.25 (m, 1H), 7.84-7.79 (m, 1H), 7.58-7.56 (m, 2H), 7.12-7.08 (m, 1H), 6.95-6.92 (m, 1H), 4.12 (t, *J* = 6.90 Hz, 2H), 3.93 (s, 3H), 1.92-1.83 (m, 2H), 1.47-1.42 (m, 2H), 1.31 (m, 8H), 0.88-0.86 (m, 3H); ¹³C NMR (75 MHz, CDCl₃): δ 165.42, 152.88, 151.74, 148.74, 147.05, 138.95, 126.41, 120.25, 119.64, 114.45, 111.97, 110.74, 69.21, 56.09, 31.80, 29.33, 29.20, 29.09, 25.93, 22.64, 21.24, 14.08; HRMS (ESI-TOF): calcd for C₂₁H₂₉N₂O₃ [M + H]⁺ 357.2173, found 357.2179.

3-(Benzyloxy)-N-(2-hydroxyethyl)-4-methoxybenzamide (2q)

White solid (65 mg, 55.7 %), M.P. 132-133 °C, ¹H-NMR (300 MHz, CDCl₃): δ 7.46-7.37 (m, 3H), 7.34-7.28 (m, 4H), 6.85-6.78 (m, 2H), 5.13 (s, 2H), 3.89 (s, 3H), 3.78 (m, 2H), 3.57 (m, 2H), 3.26 (s, 1H); ¹³C NMR (75 MHz, CDCl₃): δ 168.19, 152.57, 148.07, 136.57, 128.58, 128.04, 127.56, 126.56, 120.32, 113.05, 110.86, 71.07, 62.34, 56.04, 42.92; HRMS (ESI-TOF): calcd for C₁₇H₂₀NO₄ [M + H]⁺ 302.1387, found 302.1392.

Preparation of 3-(decyloxy)-N,4-dihydroxybenzamide (1e)

Compound **13** (50 mg) was dissolved in methanol and 10 % wet Pd/C (5 mg) were added. The mixture was stirred at room temperature for 10 h under H₂ atmosphere. As the reaction finished, the mixture was filtered, concentrated in vacuum and purified by chromatography on silica gel to give **1e**. White solid (69 mg, 89.1 %), M.P. 100-102 °C, ¹H-NMR (300 MHz, DMSO-d₆): δ 9.39 (s, 1H), 7.74 (s, 1H), 7.43-7.34 (m, 2H), 7.08 (s, 1H), 6.81-6.78 (m, 1H), 3.99 (t, *J* = 6.60 Hz, 2H), 1.75-1.68 (m, 2H), 1.42 (m, 2H), 1.26 (m, 12H), 0.88 (t, *J* = 5.40 Hz, 3H); ¹³C NMR (75 MHz, DMSO-d₆): δ 168.07, 150.20, 146.79, 125.73, 121.50, 115.21, 113.32, 68.81, 31.76, 29.52, 29.44, 29.29, 29.22, 29.18, 25.93, 22.55, 14.41; HRMS (ESI-TOF): calcd for C₁₇H₂₈NO₄ [M + H]⁺ 310.2013, found 310.2013.

Biology

In vitro ASM inhibition assay

ASM was obtained as follows. The human hepatocellular carcinoma cells (Huh 7) were grown in a medium (DMEM; 10% Gibco) at 37 °C in a humidified 5.0 % CO₂ incubator. As the cells grown to a confluence of 95 %, they were washed with phosphate-buffered saline (137 mM NaCl, 2.7 mM KCl, 10 mM Na₂HPO₄, 2 mM KH₂PO₄) and lysed in lysisbuffer (25 mM Tris-HCl, PH 7.4, 5 mM EDTA). The cells were gathered to an eppendorf tube and broken by Ultrasonic Processor with a strength of 10%. Cell debris was removed by centrifugation at 300 g for 5 min at 4 °C. The supernatant was transferred to a new eppendorf tube and the concentration of protein was detected by the BCA method.

Quantitative analysis of ASM activity was performed on 400 μg of total cellular protein extract. NBD-sphingomyelin (1 mg/mL, 4 μL) was suspended in 250 μL of enzyme buffer (100 mM sodium acetate pH 4.7, 1% Triton X-100, 40 mM CaCl₂, 100 μM ZnCl₂) and added to the protein extract. Inhibitors were added in various

concentrations in DMSO. The total volume of the reaction was adjusted to 500 μL by addition of water and incubated at 37 °C for 30 min. The reaction was stopped by addition of 800 μL of chloroform / methanol (v/v = 2:1), and phases were separated by centrifugation. 400 μL of organic phase was extracted and dried by N_2 . The products were dissolved by 30 μL chloroform and analyzed by thin layer chromatography. Inhibitory rates were determined by measuring the fluorescence intensity of produced NBD-Cers, which was quantified by the ImageJ2x software. The IC_{50} was calculated by the inhibitory rate of different compounds concentration in the GraphPad Prism 6 software. The results refer to the mean values resulting from three independent experiments.

Kinetic studies of ASM inhibition

The kinetics studies were performed according to the protocol reported above. The substrate BND-SM was dissolved with DMSO and diluted before use. The product BND-Cers was detected by HPLC. Initially different protein concentration and substrate concentration with a different reaction time were attempted to determine the reaction condition that the reaction product can be obviously detected. Next, a standard curve for NBD-Cers was established, which covering the estimated concentration spot of the product. For each concentration of the test compound, NBD-SM was used at 1.35 μM , 1.89 μM , 2.70 μM , 4.54 μM , and 13.5 μM in the reactions. The reaction was stopped after 10 min. Lineweaver-Burk plots were calculated using linear regression. Each experiment was performed in triplicate.

Ceramide generation inhibition assay

Human NIH3T3 cells were maintained in DMEM medium supplemented with 10 % fetal bovine serum under 37 °C and 5 % CO_2 . As the cells grown to a confluence of 90 %, cells were cultured with fresh medium and inhibitor was added into the cell culture. The cells were incubated for another 20 h. Quantification was carried out with the LC-MS-MS technology.

Cell apoptosis assay

Human NIH3T3 cells were maintained in DMEM medium supplemented with 10 % fetal bovine serum under 37 °C and 5 % CO_2 . Cells were seeded at 510 cells per well in 6-well plates and incubated overnight. Following, inhibitor was added into the cell culture, and incubated for another 20 h until UV irradiation. Cells without treatment of UV and inhibitors were chosen as control group. Then cells were cultured with

fresh medium during UV irradiation. The irradiation was performed at a peak emission wavelength of 315 nm, at a dose as 0.29 mW/cm^2 for 5 min. After irradiation, corresponding cells were continuously maintained at different concentration of inhibitors or solvent DMSO for another 24 h. Cells' apoptosis status was measured by flow cytometry (Becton Dickinson FACSAria III, NJ, USA).

Cytotoxic assay

Human NIH3T3 cells were maintained in DMEM medium supplemented with 10 % fetal bovine serum under $37 \text{ }^\circ\text{C}$ and 5 % CO_2 . As the cells grown overnight, inhibitor was added into the cell culture. The cells were incubated for another 24 h. Viability of cells was tested using the MTT method.

Anti-inflammation assay

Human NIH3T3 cells were maintained in DMEM medium supplemented with 10 % fetal bovine serum under $37 \text{ }^\circ\text{C}$ and 5 % CO_2 . Cells were seeded at 2×10^5 cells per well in 96-well plates and incubated overnight. Following, inhibitor was added into the cell culture, and incubated for another 20 h. Each well was added LPS to a concentration of 50 ng/mL and cells were continuously maintained for another 6 h. Then IL-6 or IL-8 was measured by ELISA method.

Notes: The authors declare no competing financial interest. These authors contributed equally to this work.

Funding: This work was supported financially by the key research & development program in Jiangsu [NO. BE2015683], by the introduction program of leading scientific and technological entrepreneurship in Nanjing [NO. 2013B14007], by the innovative research project of graduate student in Jiangsu [NO. KYLX16_1170].

References

- [1] I. Petrache, E.V. Berdyshev, Ceramide Signaling and Metabolism in Pathophysiological States of the Lung, in: D. Julius (Ed.) *Annu Rev Physiol*, 78 (2016) 463-480.
- [2] Y.A. Hannun, L.M. Obeid, The Ceramide-centric universe of lipid-mediated cell regulation: stress encounters of the lipid kind, *J Biol Chem*, 277 (2002) 25847-25850.
- [3] J.A. Chavez, S.A. Summers, A ceramide-centric view of insulin resistance, *Cell Metab*, 15 (2012) 585-594.

- [4] B. Stancevic, R. Kolesnick, Ceramide-rich platforms in transmembrane signaling, *FEBS Lett*, 584 (2010) 1728-1740.
- [5] M. Miyaji, Z.X. Jin, S. Yamaoka, R. Amakawa, S. Fukuhara, S.B. Sato, T. Kobayashi, N. Domae, T. Mimori, E.T. Bloom, T. Okazaki, H. Umehara, Role of membrane sphingomyelin and ceramide in platform formation for Fas-mediated apoptosis, *J Exp Med*, 202 (2005) 249-259.
- [6] A. Gomez-Munoz, N. Presa, A. Gomez-Larrauri, I.G. Rivera, M. Trueba, M. Ordonez, Control of inflammatory responses by ceramide, sphingosine 1-phosphate and ceramide 1-phosphate, *Prog Lipid Res*, 61 (2016) 51-62.
- [7] P.P. Sordillo, D.C. Sordillo, L. Helson, Review: The Prolonged QT Interval: Role of Pro-inflammatory Cytokines, Reactive Oxygen Species and the Ceramide and Sphingosine-1 Phosphate Pathways, *In Vivo*, 29 (2015) 619-636.
- [8] G.F. Nixon, Sphingolipids in inflammation: pathological implications and potential therapeutic targets, *Br J Pharmacol*, 158 (2009) 982-993.
- [9] C. Garcia-Ruiz, A. Morales, J.C. Fernandez-Checa, Glycosphingolipids and cell death: one aim, many ways, *Apoptosis*, 20 (2015) 607-620.
- [10] S.A. Morad, M.C. Cabot, Ceramide-orchestrated signalling in cancer cells, *Nat Rev Cancer*, 13 (2013) 51-65.
- [11] I. Petrache, V. Natarajan, L. Zhen, T.R. Medler, A.T. Richter, C. Cho, W.C. Hubbard, E.V. Berdyshev, R.M. Tudor, Ceramide upregulation causes pulmonary cell apoptosis and emphysema-like disease in mice, *Nat Med*, 11 (2005) 491-498.
- [12] L. Ciarlo, V. Manganelli, T. Garofalo, P. Matarrese, A. Tinari, R. Misasi, W. Malorni, M. Sorice, Association of fission proteins with mitochondrial raft-like domains, *Cell Death Differ*, 17 (2010) 1047-1058.
- [13] E.L. Smith, E.H. Schuchman, The unexpected role of acid sphingomyelinase in cell death and the pathophysiology of common diseases, *Faseb j*, 22 (2008) 3419-3431.
- [14] J. Kornhuber, C. Rhein, C.P. Muller, C. Muhle, Secretory sphingomyelinase in health and disease, *Biol Chem*, 396 (2015) 707-736.
- [15] J. Kornhuber, A. Medlin, S. Bleich, V. Jendrossek, A.W. Henkel, J. Wiltfang, E. Gulbins, High activity of acid sphingomyelinase in major depression, *J Neural Transm (Vienna)*, 112 (2005) 1583-1590.
- [16] V. Teichgraber, M. Ulrich, N. Endlich, J. Riethmuller, B. Wilker, C.C. De

Oliveira-Munding, A.M. van Heeckeren, M.L. Barr, G. von Kurthy, K.W. Schmid, M. Weller, B. Tummler, F. Lang, H. Grassme, G. Doring, E. Gulbins, Ceramide accumulation mediates inflammation, cell death and infection susceptibility in cystic fibrosis, *Nat Med*, 14 (2008) 382-391.

[17] S. Koka, M. Xia, Y. Chen, O.M. Bhat, X. Yuan, K.M. Boini, P.L. Li, Endothelial NLRP3 inflammasome activation and arterial neointima formation associated with acid sphingomyelinase during hypercholesterolemia, *Redox Biol*, 13 (2017) 336-344.

[18] N. Beckmann, D. Sharma, E. Gulbins, K.A. Becker, B. Edelmann, Inhibition of acid sphingomyelinase by tricyclic antidepressants and analogs, *Front. Physio.*, 5 (2014) 1-14.

[19] E. Gulbins, M. Palmada, M. Reichel, A. Luth, C. Bohmer, D. Amato, C.P. Muller, C.H. Tischbirek, T.W. Groemer, G. Tabatabai, K.A. Becker, P. Tripal, S. Staedtler, T.F. Ackermann, J. van Brederode, C. Alzheimer, M. Weller, U.E. Lang, B. Kleuser, H. Grassme, J. Kornhuber, Acid sphingomyelinase-ceramide system mediates effects of antidepressant drugs, *Nat Med*, 19 (2013) 934-938.

[20] M.J. McVey, M. Kim, A. Tabuchi, V. Srbely, L. Japtok, C. Arenz, O. Rotstein, B. Kleuser, J.W. Semple, W.M. Kuebler, Acid sphingomyelinase mediates murine acute lung injury following transfusion of aged platelets, *Am J Physiol Lung Cell Mol Physiol*, 312 (2017) L625-1637.

[21] T. Hla, A.J. Dannenberg, Sphingolipid signaling in metabolic disorders, *Cell Metab*, 16 (2012) 420-434.

[22] E. Gulbins, S. Walter, K.A. Becker, R. Halmer, Y. Liu, M. Reichel, M.J. Edwards, C.P. Muller, K. Fassbender, J. Kornhuber, A central role for the acid sphingomyelinase/ceramide system in neurogenesis and major depression, *J Neurochem*, 134 (2015) 183-192.

[23] W.Y. Ong, D.R. Herr, T. Farooqui, E.A. Ling, A.A. Farooqui, Role of sphingomyelinases in neurological disorders, *Expert Opin Ther Targets*, 19 (2015) 1725-1742.

[24] J. Riethmuller, J. Anthonysamy, E. Serra, M. Schwab, G. Doring, E. Gulbins, Therapeutic efficacy and safety of amitriptyline in patients with cystic fibrosis, *Cell Physiol Biochem*, 24 (2009) 65-72.

[25] L. Nahrlich, J.G. Mainz, C. Adams, C. Engel, G. Herrmann, V. Icheva, J. Lauer, C. Deppisch, A. Wirth, K. Unger, U. Graepler-Mainka, A. Hector, S. Heyder, M.

- Stern, G. Doring, E. Gulbins, J. Riethmuller, Therapy of CF-patients with amitriptyline and placebo--a randomised, double-blind, placebo-controlled phase IIb multicenter, cohort-study, *Cell Physiol Biochem*, 31 (2013) 505-512.
- [26] C. Adams, V. Icheva, C. Deppisch, J. Lauer, G. Herrmann, U. Graepler-Mainka, S. Heyder, E. Gulbins, J. Riethmueller, Long-Term Pulmonal Therapy of Cystic Fibrosis-Patients with Amitriptyline, *Cell Physiol Biochem*, 39 (2016) 565-572.
- [27] A. Sakata, K. Yasuda, T. Ochiai, H. Shimeno, S. Hikishima, T. Yokomatsu, S. Shibuya, S. Soeda, Inhibition of lipopolysaccharide-induced release of interleukin-8 from intestinal epithelial cells by SMA, a novel inhibitor of sphingomyelinase and its therapeutic effect on dextran sulphate sodium-induced colitis in mice, *Cell Immunol*, 245 (2007) 24-31.
- [28] A.G. Roth, D. Drescher, Y. Yang, S. Redmer, S. Uhlig, C. Arenz, Potent and selective inhibition of acid sphingomyelinase by bisphosphonates, *Angew Chem Int Ed Engl*, 48 (2009) 7560-7563.
- [29] M. Kolzer, C. Arenz, K. Ferlinz, N. Werth, H. Schulze, R. Klingenstein, K. Sandhoff, Phosphatidylinositol-3,5-Bisphosphate is a potent and selective inhibitor of acid sphingomyelinase, *Biol Chem*, 384 (2003) 1293-1298.
- [30] A.G. Roth, S. Redmer, C. Arenz, Potent inhibition of acid sphingomyelinase by phosphoinositide analogues, *Chembiochem*, 10 (2009) 2367-2374.
- [31] A.G. Roth, S. Redmer, C. Arenz, Development of carbohydrate-derived inhibitors of acid sphingomyelinase, *Bioorg Med Chem*, 18 (2010) 939-944.
- [32] S. Wetzel, W. Wilk, S. Chammaa, B. Sperl, A.G. Roth, A. Yektaoglu, S. Renner, T. Berg, C. Arenz, A. Giannis, T.I. Oprea, D. Rauh, M. Kaiser, H. Waldmann, A scaffold-tree-merging strategy for prospective bioactivity annotation of gamma-pyrones, *Angew Chem Int Ed Engl*, 49 (2010) 3666-3670.
- [33] K. Yang, B. Gao, X. Ming, Z. Huang, M. Wang, J. Dong, J. Wang, Synthesis and evaluation of xanthone derivatives as acid sphingomyelinase inhibitors: potential treatment for UV-induced skin damage, *Future Med Chem*, 9 (2017) 1887-1898.
- [34] M. Hamada, K. Iikubo, Y. Ishikawa, A. Ikeda, K. Umezawa, S. Nishiyama, Biological activities of alpha-mangostin derivatives against acidic sphingomyelinase, *Bioorg Med Chem Lett*, 13 (2003) 3151-3153.
- [35] C. Arenz, Small molecule inhibitors of acid sphingomyelinase, *Cell Physiol Biochem*, 26 (2010) 1-8.

- [36] C. Okudaira, Y. Ikeda, S. Kondo, S. Furuya, Y. Hirabayashi, T. Koyano, Y. Saito, K. Umezawa, Inhibition of acidic sphingomyelinase by xanthone compounds isolated from *Garcinia speciosa*, *J Enzyme Inhib*, 15 (2000) 129-138.
- [37] K.Z. Kan yang, Songyuan Hu, Qinlan Gu, Jinbin Dong, Jinxin Wang, Design, Synthesis and Biological Activity of Acid Sphingomyelinase Inhibitors, *Chem. J. Chin. Univ*, 36 (2015) 279-286.
- [38] A. Gorelik, K. Illes, L.X. Heinz, G. Superti-Furga, B. Nagar, Crystal structure of mammalian acid sphingomyelinase, *Nat Commun*, 7 (2016) 12196.
- [39] Z.J. Xiong, J. Huang, G. Poda, R. Pomes, G.G. Prive, Structure of Human Acid Sphingomyelinase Reveals the Role of the Saposin Domain in Activating Substrate Hydrolysis, *J Mol Biol*, 428 (2016) 3026-3042.
- [40] Y.F. Zhou, M.C. Metcalf, S.C. Garman, T. Edmunds, H. Qiu, R.R. Wei, Human acid sphingomyelinase structures provide insight to molecular basis of Niemann-Pick disease, *Nat Commun*, 7 (2016) 13082.
- [41] S.L. Schissel, G.A. Keesler, E.H. Schuchman, K.J. Williams, I. Tabas, The cellular trafficking and zinc dependence of secretory and lysosomal sphingomyelinase, two products of the acid sphingomyelinase gene, *J Biol Chem*, 273 (1998) 18250-18259.
- [42] J. Yao, H.E. Bi, Y. Sheng, L.B. Cheng, R.L. Wendu, C.H. Wang, G.F. Cao, Q. Jiang, Ultraviolet (UV) and hydrogen peroxide activate ceramide-ER stress-AMPK signaling axis to promote retinal pigment epithelium (RPE) cell apoptosis, *Int J Mol Sci*, 14 (2013) 10355-10368.
- [43] A. Charruyer, S. Grazide, C. Bezombes, S. Muller, G. Laurent, J.P. Jaffrezou, UV-C light induces raft-associated acid sphingomyelinase and JNK activation and translocation independently on a nuclear signal, *J Biol Chem*, 280 (2005) 19196-19204.
- [44] C. Pavoine, F. Pecker, Sphingomyelinases: their regulation and roles in cardiovascular pathophysiology, *Cardiovasc Res*, 82 (2009) 175-183.
- [45] H. Grassme, A. Carpinteiro, M.J. Edwards, E. Gulbins, K.A. Becker, Regulation of the inflammasome by ceramide in cystic fibrosis lungs, *Cell Physiol Biochem*, 34 (2014) 45-55.

- A ligand-based pharmacophore model was creatively generated and successfully used for development of novel direct inhibitors of ASM.
- A complex nature product was handily optimized to simple small molecules with much more potency and selectivity against ASM.
- Biological studies of **1c** demonstrated potent anti-apoptosis and anti-inflammation activity.
- **1c** could restore the ceramide concentration in the apoptosis assay, indicating the potential use of ASM inhibitor in ceramide related diseases.